

COVID-19 lockdown contribution to spring surface solar irradiance record in Western Europe

Chiel C. van Heerwaarden (chiel.vanheerwaarden@wur.nl)¹, Wouter B. Mol¹, Menno A. Veerman¹, Imme B. Benedict¹, Bert G. Heusinkveld¹, Wouter H. Knap², Stelios Kazadzis³, Natalia Kouremeti³, and Stephanie Fiedler⁴

¹*Meteorology and Air Quality Group, Wageningen University, Wageningen, The Netherlands*

²*Royal Netherlands Meteorological Institute, De Bilt, The Netherlands*

³*Physikalisch-Meteorologisches Observatorium Davos, World Radiation Center (PMOD-WRC), Davos, Switzerland*

⁴*University of Cologne, Institute of Geophysics and Meteorology, Cologne, Germany*

August 4, 2020

1 Abstract

Spring 2020 broke sun duration records across western Europe. The Netherlands recorded the highest surface irradiance since 1928, exceeding the previous extreme by 13 %, and the diffuse fraction of the total irradiance measured a record low percentage (38 %). The coinciding irradiance extreme and a reduction in anthropogenic pollution due to the COVID-19 measures triggered the hypothesis that cleaner-than-usual air contributed to the record. Based on analyses of ground-based and satellite observations and experiments with a radiative transfer model, we estimate a 1.3 % (2.3 W m^{-2}) increase in surface irradiance with respect to the 2010-2019 mean due to fewer aerosols in the atmosphere, and a 17.6 % (30.7 W m^{-2}) increase due to the exceptional dry and cloud-free weather conditions. The noticeable signal of cleaner air in the observed irradiance in western Europe suggests that larger COVID-19-related irradiance increases can be expected for more polluted regions.

2 Introduction

A large part of western Europe (Fig. 1a, hatched area) experienced exceptionally sunny and dry weather from March 23 to the end of May. Sun duration extremes were reported in the United Kingdom, Belgium, Germany, and The Netherlands [2, 3, 4, 5] paired with exceptionally deep blue skies [6]. The period had recurring weather patterns favorable for sunshine, with persistent north- to easterly flow over Western Europe or weak winds in the centre of high pressure systems. Clouds reduced daily solar irradiance on average by 22 % in 2020 with respect to clear-sky conditions, 3σ lower than the 2004-2020 mean reduction of 36 %. This resulted in a time-integrated

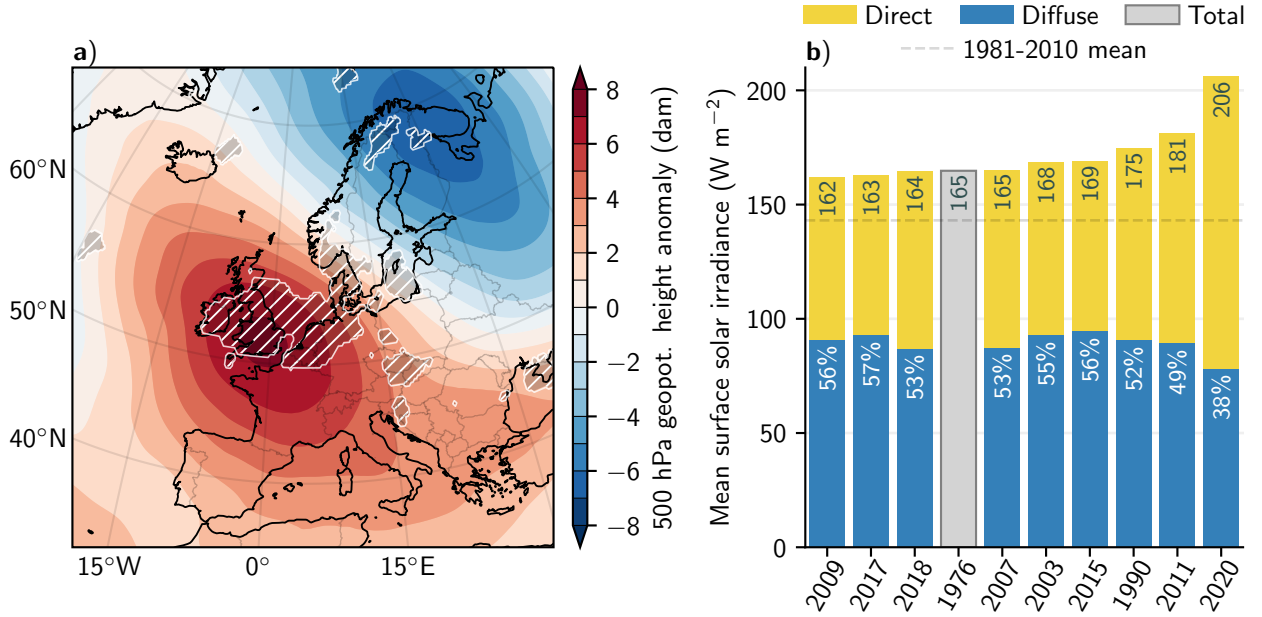


Figure 1: **Surface irradiance in spring 2020 relative to earlier years.** Figure shows **a)** 500 hPa geopotential height anomaly of 2020 spring (March, April, May) with respect to the 1981–2010 climatology, based on ERA5 reanalysis [1], hatched area indicate locations where the total irradiance in ERA5 exceeds the 1979–2019 maximum by more than 1%, and **b)** top-10 years of daily mean integrated global horizontal irradiance (GHI) since 1928 for the Veenkampen station from March 1 until May 31, partitioned into direct and diffuse. The percentages show the diffuse portion of GHI where such measurements are available. Veenkampen station was moved over a distance of 2 km in 2012, 1989 is missing from the record.

surface solar irradiance for spring (March, April, May) that was the largest ever observed at the Veenkampen station (The Netherlands) since 1928 (Fig. 1b). The daily mean irradiance sum of 206 W m^{-2} exceeded the previous record of 2011 by 25 W m^{-2} . The diffuse radiation reaching the surface was only 38% of the total solar irradiance in the period, compared to 49–58% in the other top-ten springs with high irradiance (Fig. 1).

These records all happened amid the first European wave of the COVID-19 pandemic [7, 8], during which many countries went into lockdown, leading to a reduction in anthropogenic pollution. Less traffic and industrial activity led to a 30% loss in NO_x and a 20% loss in SO_2 emissions [9, 10]. The large leap with which the irradiance records were broken made us hypothesize that the reduction in anthropogenic aerosols and contrails related to the COVID-19 lockdown are an additional driving force behind the observed irradiance extremes next to the mainly cloud-free weather.

3 Results

3.1 Time evolution of spring 2020

To test the hypothesis, we analysed data [13] from the Baseline Surface Radiation Network’s (BSRN [14]) measurement station in Cabauw, The Netherlands. This station is located in the center of the regions that reported sun duration records, and has already available observations of irradiance and aerosol optical depth (AOD) for spring 2020 (Fig. 2). The onset of the prolonged time period of fair weather on March 21 coincides

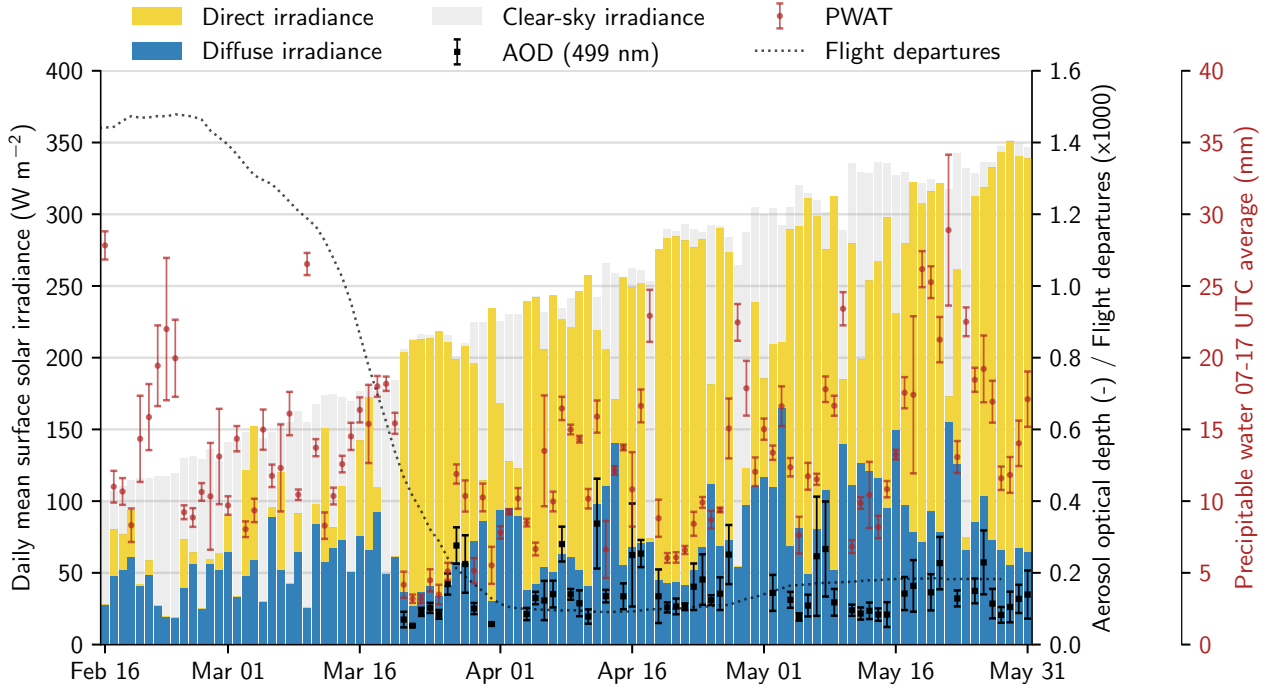


Figure 2: **Time series of relevant variables in spring 2020 in Cabauw, NL.** These include time series of measured direct and diffuse irradiance (BSRN Cabauw, NL), clear-sky global horizontal irradiance (Copernicus Atm. Monitoring Service (CAMS) McClear dataset for Cabauw), 499 nm aerosol optical depth (AOD) at Cabauw measured using a precision filter radiometer and processed at PMOD/WRC [11], daytime precipitable water (PWAT) at the grid point closest to Cabauw based on ERA5 reanalysis [1] and the weekly moving average of flight departures at (major) western Europe airports (OpenSkyNetwork COVID-19 dataset [12]). Error bars indicate daily variability ($\pm\sigma$).

with the strong drop in flight activity that marked the onset of the COVID-19 lockdown in many European countries (Fig. 2). The fair weather is reflected by the large amounts of total irradiance, i.e., direct and diffuse irradiance taken together in the observations (Fig. 2), and the large contribution of direct solar irradiance therein. Until May 31, there were only three overcast days. The surface irradiance is gradually increasing over time towards the end of May, hence the sunny days later in the period weigh more heavily in the mean shown in Fig. 1.

Especially the period of 22 to 31 March was remarkably cloud free, e.g., seen by the total irradiance equal to the clear-sky radiation, and values for diffuse irradiance are the smallest in the period. These days recorded the lowest AOD of the entire period and the lowest precipitable water in the atmosphere (Fig. 2), underlining the cleanliness and dryness of the air. Radiosonde observations of De Bilt showed strikingly low amounts of precipitable water (not shown). Based on ERA5 Reanalysis at a similar location, March 22 to 26 had on average $4.0 \pm 1.2 \text{ kg m}^{-2}$ precipitable water, far below the 1981–2019 mean of $11.5 \pm 4.2 \text{ kg m}^{-2}$ for the same period. Later, in May, multiple days had a very low AOD, including days with partial cloudiness, e.g., May 11 to 15.

3.2 Anomalies in circulation, aerosols, and contrails

In order to assess the potential impact of the COVID-19 lockdown on the irradiance extremes, and to evaluate extremes in weather versus human activity, we discuss the anomalies in atmospheric circulation (Fig. 1a), in

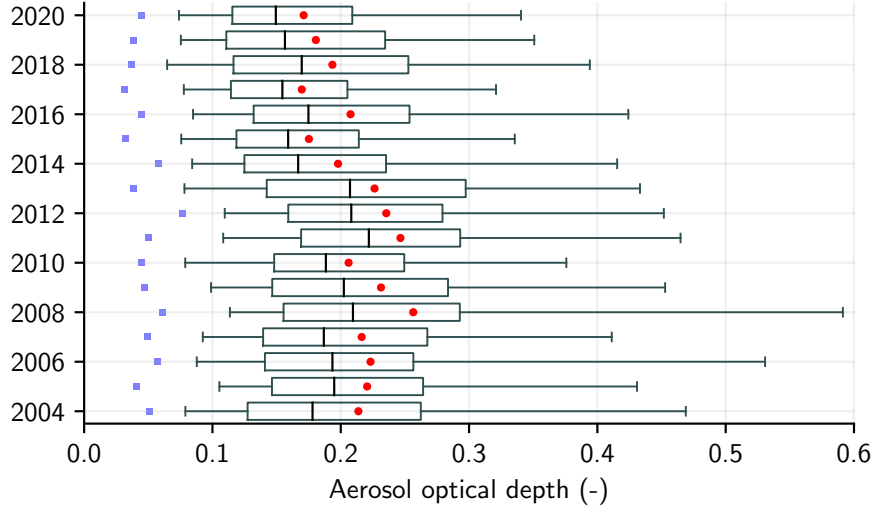


Figure 3: **Box plot of 550 nm AOD for Cabauw (NL).** Plot is based on hourly CAMS McClean [15] data for spring (March, April, May). The box-and-whisker plots span the 5th to 95th percentile, red dots are the means, blue squares are the minima. The AOD has a linear trend in the means of -0.0035 AOD per year ($r^2=0.46$, $p\text{-value}=0.0026$) and no significant trend in the minima.

AOD (Fig. 3), and in contrail formation with respect to their climatology.

The weather conditions favouring high irradiance discussed earlier are reflected by a positive anomaly in the 500-hPa geopotential height in the lockdown period centered over the south of the United Kingdom and a negative anomaly in northern Scandinavia and Russia (Fig. 1a). This pattern is typical for atmospheric blocking conditions [16], which are often drivers of heatwaves in summer and cold spells in winter [17]. In absence of temperature extremes, springtime blocking conditions attract relatively less interest [18], despite regular occurrence [19]. They are, as this study shows, a contributor to surface irradiance extremes due its related cloud-free skies, caused by its dry and sinking air masses.

Within cloud-free conditions, irradiance increases with decreasing humidity and AOD. We documented many days in 2020 with exceptionally low humidity and a low AOD (Fig. 2). To appreciate the AOD observations, we have to acknowledge the challenge in separating aerosols from homogeneous, optically thin cirrus in observations using sun photometers [20] or satellite products [21], which can result in a positively biased AOD. To avoid this difficulty and to assess a longer statistic of AOD, we use here the hourly AOD values from the CAMS aerosol product (Fig. 3), which compares well against ground-based observations over Europe [22]. Our analysis highlights that spring 2020 had the lowest median in hourly AOD since 2004. Spring 2020 was also among the springs with the lowest mean AOD, with only 2015 and 2017 being lower, but its minimum and 5th percentile values did not stand out from the statistics of hourly AODs. Therefore, the reduction in anthropogenic aerosol pollution due to the lockdowns did not lead to new extremely low hourly values of AOD, but rather to frequent hours with low AODs.

A reduction in contrail-cirrus due to the drop in flight activity (Fig. 2) is another pathway for the lockdowns to enhance surface irradiance. This is particularly true in Western Europe, which is a hot spot for contrail-cirrus, owing to a combination of high aviation activity, and suitable meteorological conditions. To obtain a

rough estimate of the effect, we compared spring 2020 to 2011 and 2015, which are both among the top-five years in terms of surface irradiance (Fig. 1b), while having contrasting AODs. Year 2011 had the highest median AOD in recent years (Fig. 3), whereas 2015 had an AOD statistic comparable to 2020 (Fig. 3). The meteorological conditions for persistent contrail-cirrus formation at 250 hPa, close to the typical flight level of 230 hPa [23], are only slightly less favourable (see Supplementary Table 1 and Fig. 5), thus we expect to observe less contrail-cirrus in 2020. Manual inspection of cirrus and contrail occurrence (see Methods) in NASA Worldview [24] imagery for the Netherlands gives results consistent with our expectation. The images showed that 2011 and 2015 had about twice as much cirrus, but with 50 % more contrail contamination, compared to 2020. Given that contrail-cirrus has a net shortwave radiative forcing in the order of -1 W m^{-2} over Western Europe [25], but can enhance diffuse irradiance with tens of percents [26, 27, 28], we speculate that the low presence of contrails contributed to the extremely low diffuse fraction that was observed in 2020. This is likely to play a small role in the total irradiance extreme compared to the generally low cloud cover in spring 2020 (Figs. 1b and 2).

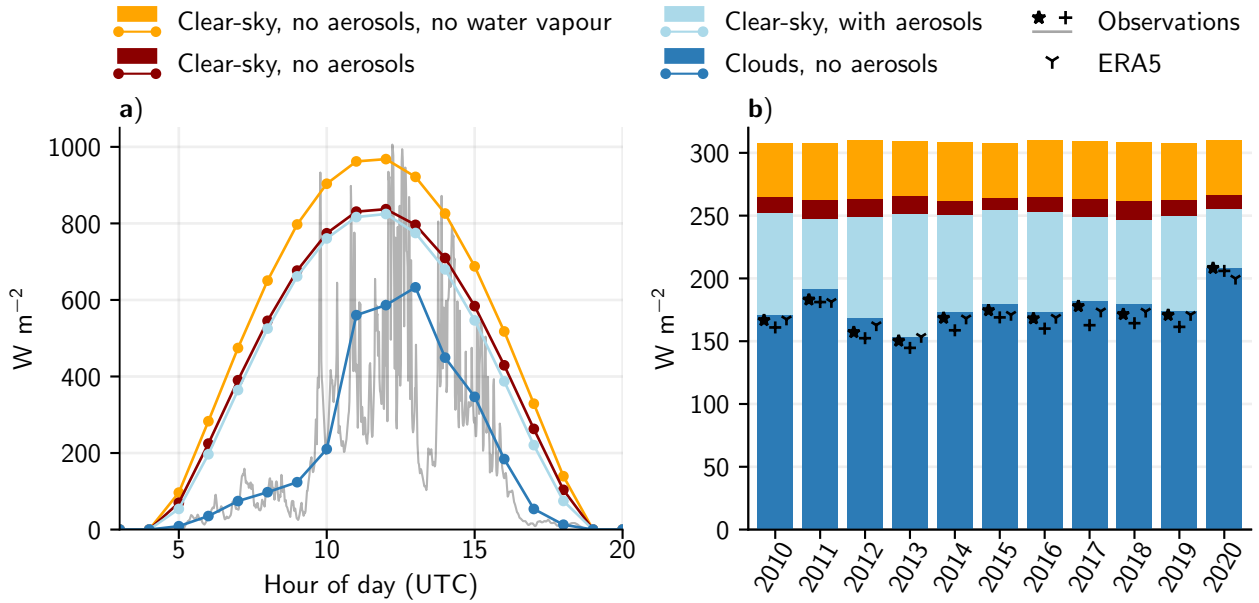


Figure 4: **Modelled surface irradiance with a radiative transfer model.** Irradiance is shown for **a)** case study of 29 April, 2020 compared against Cabauw observations, and **b)** averaged over the months March, April, and May compared against Cabauw (\star) and Veenkampen ($+$) observations and against the surface irradiance of ERA5. See Table 2 in Supplementary Table 2 for exact values corresponding to bars.

3.3 Radiative transfer modelling for interpretation of extremes

We present here estimations of i) the relative importance of different contributing factors to the extreme in surface irradiance, and ii) the anomalies in cloud radiative forcing and the direct aerosol effects. To this end, we used a contemporary radiative transfer model [29] to first reproduce the observed surface irradiance, and subsequently repeat the calculation without individual components to assess their quantitative contribution to the surface irradiance. We used the McClear clear-sky radiation product to infer the aerosol contribution [15] (see Supplementary Fig. 7 for a validation of the direct aerosol effect as a function of AOD). Further details are

given in the Methods section. The combination of the experiments with the radiative transfer model and the clear-sky data provides surface irradiance under four conditions, compared against the observations in Fig. 4:

- Experiment **dark blue** resembles the reality, but without aerosols in the atmosphere.
- Experiment **red** additionally removes the clouds.
- Experiment **orange** additionally removes the water vapour.
- Experiment **light blue** is the clear-sky product, thus without clouds but with aerosols.

We first show the modelled surface solar irradiance for a single day on 29 April in Fig. 4a for illustrating the transient behaviour of the radiative transfer model results. The experiment **dark blue** with clouds, but without aerosols closely follows the observed slowly increasing irradiance due to vanishing clouds. It confirms the ability of the model to reproduce the time series of surface irradiance (see Supplementary Fig. 6 for detailed validation). At noon, removing clouds (**red**) increases the irradiance by 250.7 W m^{-2} , and removing water vapour (**orange**) increases irradiance by a further 130.8 W m^{-2} , whereas the presence of aerosols (**light blue**) lowers the irradiance only by 12.5 W m^{-2} . Both the removal of water vapour and clouds have a larger effect on the irradiance than removing aerosols. This is not surprising due to the typically larger optical depth of clouds than aerosols, but is noteworthy in the context of the following statistical assessment.

We expand our analysis to the entire spring period for each of the past 10 years in Fig. 4b. Here, the top of each bar segment indicates the total surface irradiance for the situation indicated by its color. If clouds, aerosols, and water vapour are removed, all years have a bar of approximately equal depth, indicating that our experiment captures the essence and that leap years and year-to-year variability in atmospheric pressure, ozone, and temperature are of minor importance to the irradiance extremes in 2020. The variation over the years is comparable between the two measurement stations and is closely following the radiative transfer computations with clouds (**dark blue**), but without aerosols. The observations are consistently lower than the model simulation, consistent with the here removed aerosols. Furthermore, the Cabauw station has a consistently higher irradiance than Veenkampen, due to its closer proximity to the coast, where clouds are less common [30].

We quantify the cloud radiative effect at the surface as the difference between the experiment with clouds and the clear-sky experiment without aerosols (**dark blue** minus **red**). The irradiance increase due to the reduction in clouds is $+30.7 \text{ W m}^{-2}$ in 2020 with respect to the 2010–2019 mean cloud radiative effect of -88.6 W m^{-2} . Similarly, we quantify the aerosol effect from the difference between the clear-sky experiment without aerosols and the McClear data (**light blue** minus (**red**)). This computation indicates an increase in irradiance of $+2.3 \text{ W m}^{-2}$, with respect to the 2010–2019 mean aerosol effect of -13.0 W m^{-2} . The water vapour effect is quantified as the clear-sky experiment minus the dry experiment (**red** minus **orange**) and gives an enhancement of only $+1.5 \text{ W m}^{-2}$ with respect to the 2010–2019 mean water vapour effect of -45.4 W m^{-2} . The vapour enhancement is only the contribution to the optical properties of the clear-sky radiation, and that the most important signal of the atmospheric moisture anomaly of 2020 is tightly linked with the low cloud cover. The low humidity also affects the aerosol optical depth in the sense that less water vapour is available for condensation

on the aerosol surface keeping the aerosol optical depth smaller than in moist conditions. The quantification of the three effects highlights the relative importance of variations in cloud cover over the years in explaining the surface irradiance. It emphasizes that the sunny weather played the most important role in setting the 2020 record in surface irradiance, while the reduced emission of anthropogenic aerosols is of smaller importance, to the extent that even without the reduction the irradiance record had occurred.

4 Discussion

During the exceptionally sunny spring in western Europe amid the COVID-19 pandemic in 2020, The Netherlands received the most solar radiation at the surface since the start of the measurements in 1928 and never experienced so little scattering of light (Fig. 1b). The particularly dry atmosphere (Fig. 2) and weather patterns favouring sunny weather (Fig. 1a) led to fewer clouds than in previous years. Based on radiative transfer calculations, we estimated the relative contributions of aerosols, water vapour, and clouds and argue that the latter is the dominant contributor to the new irradiance extreme (Fig. 4), while the impact of COVID-19 lockdowns is at least an order of magnitude less.

Our analysis separates the contribution of aerosols from that of clouds, allowing us to estimate the irradiance increase in 2020 due to a reduction in the direct aerosol effect at 2.3 W m^{-2} . Measured by the median, spring 2020 was the cleanest on record in The Netherlands since 2004 (Fig. 3b). The trend of $-3.5 \cdot 10^{-3} \text{ y}^{-1}$ in the means continues the generally decreasing trend in anthropogenic aerosol emissions in Europe, an effect known as brightening from earlier studies [31, 32, 33]. Today's already low anthropogenic aerosol emissions in Europe are expected to stay small or even further decrease in the future [34], which could enable even larger irradiance extremes. Changes in future circulation and related cloudiness could enforce or counter new extremes, but the uncertainty in projections thereof [18, 35] must be reduced before more definitive statements on future irradiance extremes can be made.

Further effects of the aerosol removal are possible, including rapid adjustments of clouds and circulation to associated temperature changes and aerosol effects on cloud microphysical processes, but these can not be quantitatively assessed with the model used here. Qualitatively, a reduction in anthropogenic aerosols could for instance reduce the cloud albedo and enhance the surface irradiance in cloudy conditions, but the uncertainty in the quantification of aerosol-cloud interactions is still large [36]. If we account for additional aerosol effects, the impact of the reduced anthropogenic aerosols due to the lockdown is expected to be larger than our estimate of the instantaneous clear-sky radiative effects of the aerosol removal. Despite all uncertainty, larger effects of aerosol reductions from COVID-19 lockdowns are expected for typically more polluted regions than western Europe. With the current spread of the pandemic in strongly polluted regions, more data to test our expectation will become available in the near future.

Author contributions

CvH, WM, and MV designed the study. WM performed the data analysis of the observations. MV performed the radiative transfer model experiments. CvH, WM, MV, IB and SF interpreted the results. CvH, WM, MV, and SF wrote the manuscript. BH, WK, SK, and NK provided observational data and expertise thereof. All authors read the final manuscript and provided feedback.

Acknowledgments

CvH, WM, MV, and BH acknowledge funding from the Dutch Research Council (NWO) (grant: VI.Vidi.192.068). SF acknowledges the funding of the Hans-Ertel-Centre for Weather Research by the German Federal Ministry for Transportation and Digital Infrastructure, (grant: BMVI/DWD 4818DWDP5A).

5 Methods

5.1 Cirrus and contrail-contamination estimation

Effects of aviation are estimated by comparing two top-5 irradiance years with relatively high and low AOD with 2020, hence the choice of 2011 and 2015. Environmental conditions favourable for persistent contrails, namely a low air temperature at flight level [23], and often occurring supersaturation with respect to ice [37, 38], are quantified using ERA5 reanalysis for a domain covering approximately The Netherlands at 250 and 300 hPa. Cirrus occurrence and whether it is contaminated by contrails is manually counted by looking at high resolution satellite images from Terra and Aqua MODIS, available on the NASA Worldview website [24]. The inspected area covers the Netherlands and closely neighbouring regions (Belgium, western Germany and part of the North Sea). This area is part of the irradiance extreme coverage (Fig. 3 and helps offset the fact only two images close to noon per day are available. Only cirrus and contrails optically thick enough to be detectable by eye can be counted, anything that is too thin to detect is assumed to have only a very small impact on irradiance. Contrail-contamination is counted when there is cirrus with five or more linear (typically overlapping) or unnatural looking (dispersed) condensation trails present. See Supplementary Fig. 5 for a clear example.

5.2 Radiative transfer modelling

We used the Radiative Transfer for Energetics and RRTM for General circulation model applications—Parallel (RTE+RRTMG) [29] to reproduce the surface irradiance observations at Cabauw, The Netherlands for spring 2020 (March, April, May) in order to construct Fig. 4. The computation requires hourly atmospheric profiles of pressure, temperature, water vapour, liquid water, ice, cloud cover, cloud liquid water, cloud ice, and ozone at a $0.25 \times 0.25^\circ$ grid resolution taken from the ERA5 reanalysis [1]. We used the data on 37 pressure levels instead of the 137 native model levels, but the vertical integrals are approximately conserved. We assume i)

clouds to be horizontally homogeneous within one grid cell, ii) that adjacent cloud layers have overlap, iii) that the spatial correlation between two clouds layers decreases exponentially (using a decorrelation length of 2 km) with increasing vertical distance between the layers, and iv) that separated cloud layers have random overlap. To obtain a statistical distribution of the cloud fields, we sampled 100 vertical profiles, calculated radiative fluxes for each profile and subsequently averaged the surface irradiance. To infer the effect of aerosols, we used the surface irradiance product of the Copernicus Atmosphere Monitoring service (CAMS) McClear Clear-Sky Irradiating service [15].

6 Data availability

All data used in this manuscript is either available from public sources or included with this manuscript. Public sources are cited in the manuscript. Data that is non-public will be made publicly available after paper is accepted and a DOI will be attached. Until then a zip file is included with the manuscript.

References

- [1] Hersbach, H. *et al.* The ERA5 global reanalysis. *Quarterly Journal of the Royal Meteorological Society* **146**, 1999–2049 (2020).
- [2] Madge, G. May 2020 becomes the sunniest calendar month on record. *United Kingdom Met Office* (2020). URL <https://www.metoffice.gov.uk/about-us/press-office/news/weather-and-climate/2020/2020-spring-and-may-stats>.
- [3] DWD. German weather in spring 2020. *Deutsche Wetter Dienst* (2020). URL https://www.dwd.de/DE/presse/pressemittelungen/DE/2020/20200529_deutschlandwetter_fruehjahr2020_news.html.
- [4] KNMI. Sunniest spring since start of measurements. *Royal Dutch Meteorological Institute* (2020). URL <https://www.knmi.nl/over-het-knmi/nieuws/zonnigste-lente-sinds-het-begin-van-de-metingen>.
- [5] KMI. A dry and exceptionally sunny spring. *Royal Meteorological Institute* (2020). URL <https://www.meteo.be/nl/klimaat/klimatologisch-overzicht/2020/lente>.
- [6] Knap, W. & Meirink, J. F. Uitzonderlijk blauwe voorjaarsluchten. *Royal Netherlands Meteorological Institute* (2020). URL <https://www.knmi.nl/over-het-knmi/nieuws/uitzonderlijk-blauwe-voorjaarsluchten>.
- [7] COVID-19 dashboard by the Center for Systems Science and Engineering (CSSE) at Johns Hopkins University (JHU). URL <https://coronavirus.jhu.edu/map.html>. Accessed: 2020-07-21.
- [8] European Centre for Disease Prevention and Control, COVID-19 pandemic. URL <https://www.ecdc.europa.eu/en/covid-19-pandemic>. Accessed: 2020-07-21.

- [9] Forster, P. M. *et al.* Current and future global climate impacts resulting from COVID-19. *Nature Climate Change* (2020).
- [10] Muhammad, S., Long, X. & Salman, M. COVID-19 pandemic and environmental pollution: A blessing in disguise? *Science of The Total Environment* **728**, 138820 (2020).
- [11] Kazadzis, S., Kouremeti, N., Nyeki, S., Gröbner, J. & Wehrli, C. The world optical depth research and calibration center (WORCC) quality assurance and quality control of GAW-PFR AOD measurements. *Geoscientific Instrumentation, Methods and Data Systems* **7**, 39–53 (2018).
- [12] Schafer, M., Strohmeier, M., Lenders, V., Martinovic, I. & Wilhelm, M. Bringing up OpenSky: A large-scale ADS-b sensor network for research. In *IPSN-14 Proceedings of the 13th International Symposium on Information Processing in Sensor Networks* (IEEE, 2014).
- [13] Knap, W. Basic and other measurements of radiation at station Cabauw (2020-02) (2020). URL <https://doi.pangaea.de/10.1594/PANGAEA.913473>.
- [14] Driemel, A. *et al.* Baseline surface radiation network (BSRN): structure and data description (1992-2017). *Earth System Science Data* **10**, 1491–1501 (2018).
- [15] Gschwind, B. *et al.* Improving the McClear model estimating the downwelling solar radiation at ground level in cloud-free conditions – McClear-v3. *Meteorologische Zeitschrift* **28**, 147–163 (2019).
- [16] Folland, C. K. *et al.* The summer North Atlantic Oscillation: Past, present, and future. *Journal of Climate* **22**, 1082–1103 (2009).
- [17] Pfahl, S. & Wernli, H. Quantifying the relevance of atmospheric blocking for co-located temperature extremes in the Northern Hemisphere on (sub-) daily time scales. *Geophysical Research Letters* **39** (2012).
- [18] Woollings, T. *et al.* Blocking and its response to climate change. *Current climate change reports* **4**, 287–300 (2018).
- [19] Brunner, L., Hegerl, G. C. & Steiner, A. K. Connecting atmospheric blocking to European temperature extremes in spring. *Journal of Climate* **30**, 585–594 (2016).
- [20] Chew, B. N. *et al.* Tropical cirrus cloud contamination in sun photometer data. *Atmospheric Environment* **45**, 6724 – 6731 (2011). URL <http://www.sciencedirect.com/science/article/pii/S1352231011008375>.
- [21] Kaufman, Y. J. *et al.* A critical examination of the residual cloud contamination and diurnal sampling effects on modis estimates of aerosol over ocean. *IEEE Transactions on Geoscience and Remote Sensing* **43**, 2886–2897 (2005).
- [22] Gueymard, C. A. & Yang, D. Worldwide validation of cams and merra-2 reanalysis aerosol optical depth products using 15 years of aeronet observations. *Atmospheric Environment* **225**, 117216 (2020).

- [23] Burkhardt, U. & Kärcher, B. Global radiative forcing from contrail cirrus. *Nature Climate Change* **1**, 54–58 (2011).
- [24] NASA Worldview. URL <https://worldview.earthdata.nasa.gov>. Accessed: 2020-07-25.
- [25] Stuber, N., Forster, P., Rädcl, G. & Shine, K. The importance of the diurnal and annual cycle of air traffic for contrail radiative forcing. *Nature* **441**, 864–867 (2006).
- [26] Feister, U. & Shields, J. Cloud and radiance measurements with the VIS/NIR Daylight Whole Sky Imager at Lindenberg (Germany). *Meteorologische Zeitschrift* **14**, 627–639 (2005).
- [27] Gueymard, C. A. Temporal variability in direct and global irradiance at various time scales as affected by aerosols. *Solar Energy* **86**, 3544 – 3553 (2012). URL <http://www.sciencedirect.com/science/article/pii/S0038092X12000291>. Solar Resources.
- [28] Weihs, P. *et al.* Potential impact of contrails on solar energy gain. *Atmospheric Measurement Techniques* **8**, 1089–1096 (2015).
- [29] Pincus, R., Mlawer, E. J. & Delamere, J. S. Balancing accuracy, efficiency, and flexibility in radiation calculations for dynamical models. *Journal of Advances in Modeling Earth Systems* **11**, 3074–3089 (2019).
- [30] KNMI climatology overviews. <https://www.knmi.nl/nederland-nu/klimatologie/geografische-overzichten/archief/maand/sq>. Accessed: 2020-07-27.
- [31] Wild, M., Ohmura, A., Gilgen, H. & Rosenfeld, D. On the consistency of trends in radiation and temperature records and implications for the global hydrological cycle. *Geophysical Research Letters* **31**, L11201 (2004).
- [32] Wild, M. *et al.* From dimming to brightening: Decadal changes in solar radiation at earth’s surface. *Science* **308**, 847–850 (2005).
- [33] Wild, M. Enlightening Global Dimming and Brightening. *Bulletin of the American Meteorological Society* **93**, 27–37 (2012).
- [34] Fiedler, S. *et al.* First forcing estimates from the future CMIP6 scenarios of anthropogenic aerosol optical properties and an associated Twomey effect. *Geoscientific Model Development* **12**, 989–1007 (2019).
- [35] Bony, S. *et al.* Clouds, circulation and climate sensitivity. *Nature Geoscience* **8**, 261–268 (2015).
- [36] Bellouin, N. *et al.* Bounding global aerosol radiative forcing of climate change. *Reviews of Geophysics* **58**, e2019RG000660 (2020).
- [37] Jensen, E. J. *et al.* Environmental conditions required for contrail formation and persistence. *Journal of Geophysical Research: Atmospheres* **103**, 3929–3936 (1998).
- [38] Lee, D. S. *et al.* Aviation and global climate change in the 21st century. *Atmospheric Environment* **43**, 3520–3537 (2009).

Supplementary material

The supplementary material contains a series of figures and tables with additional material to complement and validate the analyses and radiative transfer model computations that are discussed in the main text. All items are referenced from the main text.

Table 1: Percentage of days in March, April and May with visible cirrus and the percentage those days which are visibly contaminated with contrails. Based on Terra and Aqua MODIS imagery on NASA Worldview [24].

	2011	2015	2020
Cirrus	51	60	30
Contrail contaminated	62	59	42

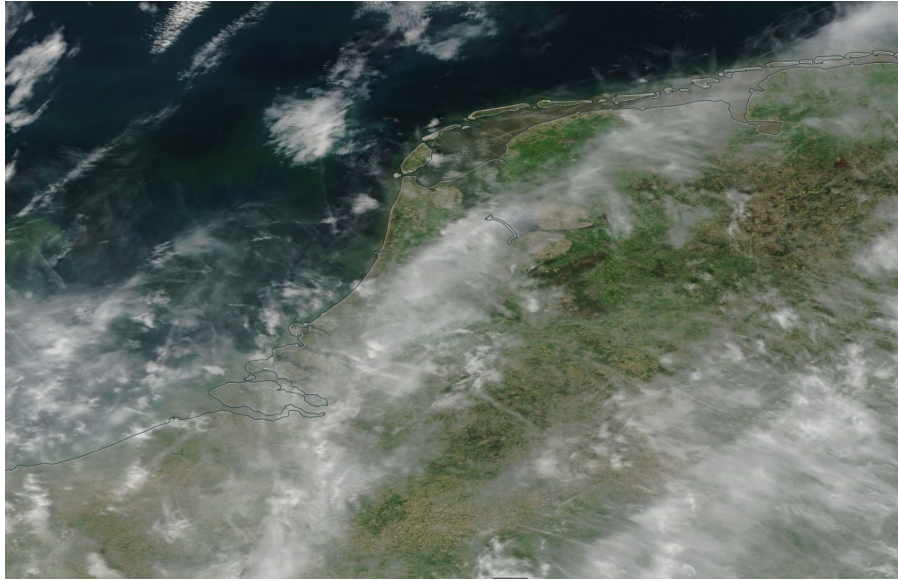


Figure 5: Example from NASA Worldview of cirrus that contains (and is therefore enhanced in coverage and optical thickness) contrails, from narrow and straight ones to older and more dispersed. The date of this image is 11 May 2015.

Table 2: Surface irradiance per experiment in units of W m^{-2} for the period March, April, May for each of the years 2010–2020.

	2010	2011	2012	2013	2014	2015	2016	2017	2018	2019	2020
Dry (orange)	308.2	308.1	310.0	309.1	308.6	307.7	309.9	309.4	308.5	307.8	310.1
Clear (red)	264.6	262.4	263.4	265.3	261.9	263.8	264.8	262.9	261.4	262.6	266.2
McClear (light blue)	252.1	247.1	249.0	251.6	250.7	254.3	253.2	249.2	246.6	249.3	255.4
Clouds (dark blue)	170.5	191.9	168.5	153.4	173.5	179.6	173.6	182.1	179.9	174.2	208.3

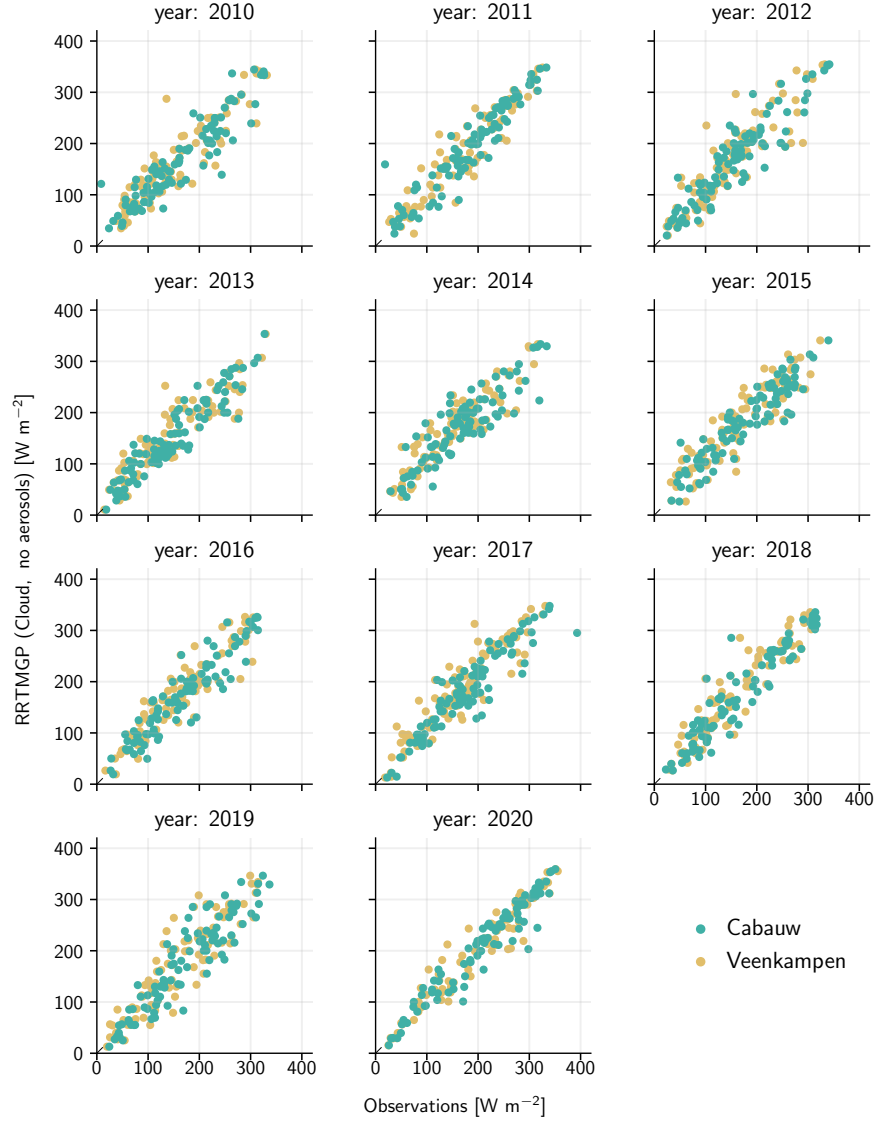


Figure 6: Daily mean surface irradiances based on RTE+RRTMGP simulation with clouds but without aerosols against daily mean surface irradiances based on observations at Cabauw and at Veenkampen. Each year is shown in a single panel and the data points represent all individual days in March, April and May.

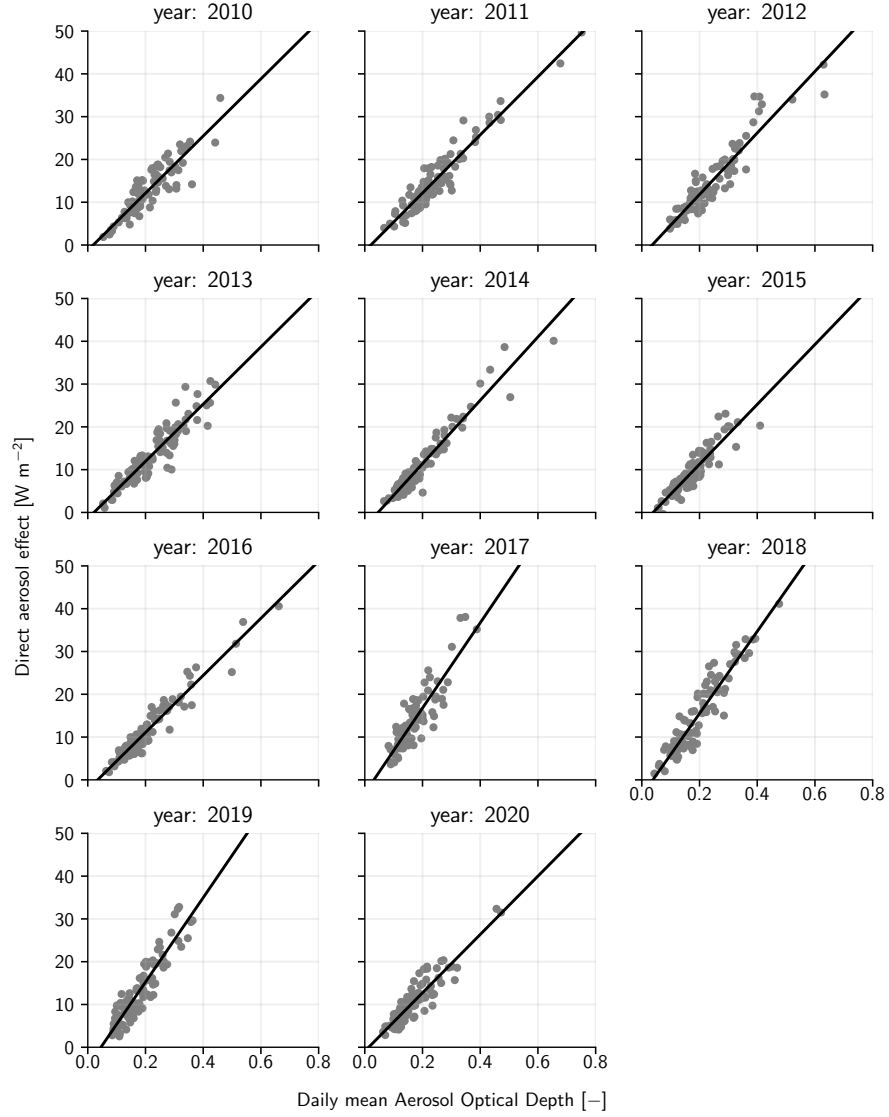


Figure 7: Daily mean direct aerosol effect, computed as the difference between the clear-sky RTE+RRTMGP simulation without clouds and aerosols and the McClean clear-sky product, against daily mean aerosol optical depth. Each year is shown in a single panel and the data points represent all individual days in March, April and May. The black lines indicate the linear trend.